THE ASTROPHYSICAL JOURNAL, 381:361–372, 1991 November 10

A PHOTOIONIZATION MODEL FOR THE OPTICAL LINE EMISSION FROM COOLING FLOWS

MEGAN DONAHUE[1] AND G. MARK VOIT[2]
Center for Astrophysics and Space Astronomy, Department of Astrophysical, Planetary, and Atmospheric Sciences, University of Colorado
Received 1990 September 19; accepted 1991 May 15

ABSTRACT

We present the detailed predictions of a photoionization model previously outlined in Voit and Donahue to explain the optical line emission associated with cooling flows in X-ray emitting clusters of galaxies. In this model, EUV/soft X-ray radiation from condensing gas photoionizes clouds that have already cooled. We discuss the energetics and specific consequences of such a model, as compared to other models put forth in the literature. We also discuss the consequences of magnetic fields and cloud-cloud shielding. Our results illustrate how varying the individual column densities of the ionized clouds can reproduce the range of line ratios observed and strongly suggest that the emission-line nebulae are self-irradiated condensing regions at the centers of cooling flows.

Subject headings: galaxies: clustering — galaxies: intergalactic medium — galaxies: X-rays

1. INTRODUCTION

In this paper, we present a theoretical model which explains the optical filamentation associated with cooling flows in many X-ray emitting clusters of galaxies. Our model relates the observed optical properties of the filaments to the actual physical processes, such as accretion and thermal instability, occurring in the cluster gas. The thesis of the model is that the optically emitting filaments are powered by the radiation emitted by a confining bath of X-ray and EUV emitting gas (see Voit & Donahue 1990, hereafter Paper I).

In § 2, we discuss the observed characteristics of cooling flows in clusters of galaxies, and in § 3, we briefly review previous models for generating the optical emission such as repressurizing shocks and photoionization by a central source. Our model is described in § 4, and the results are presented in § 5, where we show that the X-ray to optical conversion ratio can be quite high and that varying only the column density of the photoionized cloudlets shifts the optical line ratios through their observed range. In § 6, we compare our results to the observations and discuss their implications. The final section summarizes our findings.

2. OBSERVATIONS

Here we briefly outline the observational background of cooling flows in clusters of galaxies, seeking clues as to what might power the optical emission. We describe the general properties of X-ray emitting clusters of galaxies and of the optical filaments associated with some of these clusters.

2.1. *X-Ray Properties of Clusters of Galaxies*

The X-ray emitting gas in clusters of galaxies is very luminous, (10^{43}–10^{45}) ergs s^{-1}, with an X-ray spectral shape characteristic of thermal bremsstrahlung at 10^{7-8} K plus some high-ionization iron lines (see Mushotzky et al. 1978; Mitchell et al. 1979; Henriksen & Mushotzky 1986; Henriksen 1985). Emission modeling of these clusters is generally consistent with the assumption that gas is bound in the gravitational potential of a cluster of galaxies, with a 200 to 500 kpc core radius, roughly the same as that of the galaxies in the clusters. The radiative cooling time of this gas can be computed from the temperatures and densities derived from X-ray observations. Without some source of additional heating, the hot gas will eventually radiate away its energy and settle into the potential well, forming a cooling flow if the central cooling time is shorter than a typical cluster age or Hubble time (Fabian & Nulsen 1977; Cowie & Binney 1977; Fabian, Nulsen, & Canizares 1984). A complete review of this topic can be found in Sarazin (1988).

Many X-ray emitting clusters appear to have cooling flows: between 40% (Arnaud 1988) and 80% (Stewart et al. 1984; Edge & Stewart 1991) of all clusters have cooling times shorter than the Hubble time within some small radius. The existence of cooling flows is supported by observations of X-ray surface brightness profiles that are peaked in the center (e.g., Fabian et al. 1981), by measurements of inverted temperature gradients (e.g., Gorenstein et al. 1977), by observations of central X-ray surface brightnesses and temperatures that imply cooling times much less than the Hubble time (Canizares, Stewart, & Fabian 1983; Stewart et al. 1984), and by *Einstein* FPCS detections of Fe XVII and O VIII emission, representative of 10^{6-7} K gas, thus implying cooling (Canizares, Markert, & Donahue 1988; Canizares et al. 1979, 1982). The mass inflow rates ($\dot{M}$) derived from these observations are high (1–500 $M_\odot$ yr^{-1}) and often appear to decrease with decreasing radius (Thomas, Fabian, & Nulsen 1987; White & Sarazin 1988). In other words, the amount of mass seen cooling and emitting X-rays at a radius of 250 kpc seems greater than the amount of mass cooling and emitting at smaller radii ($\sim$50 kpc or so).

2.2. *Optical Properties*

A large proportion (perhaps $\sim$70% according to Heckman et al. 1989, hereafter HBvM) of the clusters which are thought to contain cooling flows also contain extended Hα line emission in their cores (Cowie et al. 1983; Hu, Cowie, & Wang 1985; Heckman 1981; Johnstone, Fabian, & Nulsen 1987, hereafter JFN1987; Baum 1987; Romanishin & Hintzen 1988;

[1] The Observatories of the Carnegie Institution of Washington, 813 Santa Barbara Street, Pasadena, CA 91101.
[2] Caltech, Theoretical Astrophysics, Mail Code 130-33, Caltech, Pasadena, CA 91125.

HBvM). These studies have revealed a correlation between the presence of a cooling flow, as determined from X-ray data, and the presence of extended Hα line emission. Other strong optical lines detected in cooling flows are [N II], [O I], [O II], and [S II] (HBvM; JFN1987). This optical emission is more centrally concentrated than the X-ray emission, typically extending to radii of approximately 10 kpc, but a nearby cluster cooling flow (NGC 1275 in the Perseus cluster) is a spectacular example of filamentation extending to a radius of 100 kpc (see Minkowski 1957; Lynds 1970). Typical Hα luminosities are 10^{41} to 10^{42} ergs s^{-1}. One of the major puzzles associated with this optical luminosity is its strength: if the Hα luminosity is created by the cooling flow, and we assume that each H atom in the flow recombines once (simple cooling) or three times (shocks), then the $\dot{M}$ derived from the Hα luminosity is 10–100 times greater than that derived from X-ray data. This puzzle is called the "H-rec" problem in the literature (e.g., JFN1987; HBvM). Additionally, not all clusters with X-ray derived cooling flows have Hα emission (e.g., A2029). This discrepancy cannot be explained by the errors inherent in the determination of $\dot{M}$ from X-ray surface brightness profiles, so a model of this emission should also explain why some ($\sim$30%) cooling flows do not show optical line emission.

Some evidence exists for two classes of emission-line system (HBvM) in cooling flows, tentatively named "class I" and "class II," distinguished by their separation in line-ratio diagrams (see Baldwin, Phillips, & Terlevich 1981). The class I objects (A262, M87, and A2052) have strong [N II]/Hα and [S II]/Hα but weak [O I]/Hα relative to those in class II (NGC 1275, PKS 0745−191, Hydra A, A1795, and A2597). Class I objects also have lower X-ray and Hα luminosities, smaller optical nebulae, and lower $\dot{M}$. The class II objects' line ratios are generally better fit by shock and photoionization models; however, the ratios of class I objects are not fit by either.

3. OPTICAL EMISSION-LINE MODELS

In the following paragraphs we discuss the difficulties associated with the various models proposed to explain the optical line ratios and luminosities in cooling flows.

3.1. *Low-Velocity Shocks*

Low-velocity (90–110 km s^{-1}) shocks (Shull & McKee 1979) approximately match some of the line ratios observed in class II clusters, but underestimate the [N II]/Hα ratio seen in class I clusters. Low-velocity shocks also require large mass processing rates. If we use values from Shull & McKee (1979), (corrected for a factor of 2 error in $I(\mathrm{H}\beta)$; Shull 1990, private communication) the effective area of shocked gas is

$$A_{\mathrm{shock}} = \frac{L_{\mathrm{H}\alpha}}{4\pi I(\mathrm{H}\alpha)} \quad (1)$$

$$= (4 \times 10^{45}\ \mathrm{cm}^2) L_{42} \quad (2)$$

where $L_{42} = L_{\mathrm{H}\alpha}/10^{42}$ ergs s^{-1}, $L_{\mathrm{H}\alpha}$ is the Hα luminosity, and $I(\mathrm{H}\alpha)$ is the intensity of Hα radiation from a 100 km s^{-1} shock. The mass processing rate in such shocks can be estimated using:

$$\dot{M} = \bar{m}_{\mathrm{H}}\, n_{\mathrm{H}}\, v_s\, A_{\mathrm{shock}} \quad (3)$$

$$= (1.5 \times 10^4\ M_\odot\ \mathrm{yr}^{-1}) v_{100}\, L_{42}\, n_{10} \quad (4)$$

where $\bar{m}_{\mathrm{H}}$ is the mean mass per H atom, $n_{\mathrm{H}} = n_{10}$ (10 cm^{-3}) is the total hydrogen density in the preshock gas, and $v_s = v_{100}$ (100 km s^{-1}) is the shock velocity. The $\dot{M}$ required to produce the observed Hα luminosities in the central 10 kpc is over one order of magnitude higher than that estimated from the X-ray surface brightness of an entire cluster.

3.2. *Photoionization by a Central Source*

HBvM and Johnstone & Fabian (1988) rule out large-scale photoionization by a strong central source in the majority of cases where line-ratio variations have been studied in detail. These studies reveal a lack of radial variation in the emission-line ratios, which would have indicated a radial dilution of ionizing emission from a hypothetical central source (Cygnus A and 3C 295 are the exceptions). In addition, power-law photoionization models (e.g., Ferland & Netzer 1983) also do not reproduce the high [N II]/Hα ratios seen in class I filaments (HBvM).

3.3. *Hot Stars*

Recent observations of central cluster galaxies showing excess blue light (Romanishin & Hintzen 1989; McNamara & O'Connell 1989) and a small 4000 Å break (JFN1987) have indicated the presence of hot stars. However, H II regions illuminated by hot stars produce [N II]/Hα ratios too small by factors of at least 3 to 6 and [O I]/Hα too small by factors of 3 to 30 to explain the observed line ratios (Johnstone & Fabian 1988). The [O III]/Hβ ratio is not such a problem since this ratio is highly sensitive to the temperature of the central star in the H II region and can vary by one order of magnitude (see Osterbrock 1989).

3.4. *High-Velocity Shocks*

Binette, Dopita, & Tuohy (1985) model high-velocity, low-density radiative shocks in which radiation from cooling, shocked gas illuminates the cooler, downstream condensed gas. Since the postshock gas is heated to temperatures high enough to produce soft X-rays, the physics of our model and theirs are quite similar. Some of their models (e.g., B60) approximate the observed line ratios, but like low-velocity shocks, they require huge mass flows to reproduce the line luminosities ($\dot{M} \sim 2.9 \times 10^3\ M_\odot\ \mathrm{yr}^{-1}\ L_{42}$, where $L_{42} = L_{\mathrm{H}\alpha}/10^{42}$ ergs s^{-1}). The model that comes closest to ours is B70, which can produce large Hα luminosities with smaller $\dot{M}$ ($\dot{M} \sim 200\ M_\odot\ \mathrm{yr}^{-1}\ L_{42}$) but does not reproduce the observed line ratios. Their shock models tend to overproduce [O I] relative to Hα due to a lower incident energy flux (which reduces the effective ionization parameter of their model relative to ours) and to overproduce [N II] relative to Hα because their models cut off when the fractional ionization is less than 1%, thus neglecting nonthermal excitation of Hα by X-ray photoelectrons in high column density clouds.

3.5. *Photoionization by the Cooling Gas*

Johnstone & Fabian (1988) and JFN1987 briefly discuss a model similar to ours, in which the ionized region is $\lesssim 10^{18}$ cm^{-2} thick. Without giving the results of their models, they state that they can reproduce the observed line ratios, but not the requisite luminosities. However, as the success of our model demonstrates, their dismissal of this mechanism may have been too hasty. We investigate a key possibility that they do not, namely, that in a special minority of clusters, a significant fraction of the X-ray derived $\dot{M}$ flows into the line-emitting region and condenses into much thicker clouds.

4. A PHOTOIONIZATION MODEL FOR SELF-IRRADIATED CONDENSING REGIONS

In this section we present the details of a photoionization model for the optical filaments in clusters of galaxies. First, we will present the general arguments for believing that the line emission arises from EUV/soft X-ray self-irradiation of cooling condensations. Next, we discuss a simple analytical model for the structure of a central condensing region. Then, we will describe the photoionization model and estimate the expected Hα luminosities and surface brightnesses.

4.1. *Why EUV/Soft X-Ray Irradiation?*

One of the main clues suggesting that EUV and soft X-ray photons photoionize the filaments is that the low-ionization forbidden lines ([O II], [N II]) are extremely strong with respect to Hα, especially in HBvM class I objects. Since these lines are produced via collisional excitation, while Hα is produced via recombination, these ratios indicate that the heating per ionization is high. This is typical of EUV photoionization where the average photon energy is high enough to heat the gas substantially with every ionization.

In addition, Hα/Hβ ratios powered by an X-ray/EUV dominated spectrum exceed Case B ratios. Typical Hα/Hβ ratios in a high column-density X-ray photoionized gas hover near 4.0, while UV-driven Case B recombination gives Hα/Hβ $\sim$ 2.86 for $T = 10^4$ K (Ferland & Osterbrock 1985). The Perseus (A 426, NGC 1275) Hα/Hβ ratio is observed to be $\sim$4.77 for the low-velocity system (Kent & Sargent 1979), and this large value has been attributed to reddening intrinsic to the cluster. However, it may not be necessary to cite excessive reddening since a high Hα/Hβ ratio is a natural consequence of EUV/X-ray photoionization.

The fact that the energy content of the cooling gas is sufficient to power the optical luminosities provides another clue (HBvM). HBvM compare cluster surface brightnesses in X-rays to those in optical emission lines and find that if the X-rays can be efficiently absorbed, the energy in the X-ray gas *local to the filaments* is sufficient to power the optical lines. The mechanism we present below efficiently converts the high-energy photons radiated by the gas into optical lines.

The ionization state of the gas also suggests that the condensing region is self-irradiated. Two ionization parameters commonly used in the literature are: U, the ratio of the number density of ionizing photons to the total number density of hydrogen, defined by

$$U = \frac{\mathscr{F}_E f_i}{c\langle E\rangle n_{\rm H}}, \tag{5}$$

where $\mathscr{F}_E$ is the energy flux at the surface of the filaments, f_i is the fraction of the energy flux above 13.6 eV, $\langle E\rangle$ is the mean ionizing photon energy, and $n_{\rm H}$ is the total (ionized and neutral) number density of hydrogen; and Ξ, the ratio of the radiation pressure to the gas pressure, defined by

$$\Xi = \frac{P_{\rm rad}}{P_{\rm gas}} = \frac{\mathscr{F}_E f_i}{c\chi n_{\rm H} k T_{\rm fil}}, \tag{6}$$

where χ is the number of gas particles per hydrogen atom (neutral and ionized), and $T_{\rm fil}$ is the temperature of the filaments. In a self-irradiated cooling region, the $\mathscr{F}_E$ incident on a condensate will be $\sim P_{\rm hot} v_{\rm hot}$ where $P_{\rm hot}$ is the pressure of the hot gas and $v_{\rm hot}$ is the rate at which it flows into the condensing region (Paper I). If the cool gas is in pressure equilibrium with the hot gas, then $\Xi \sim v_{\rm hot}/c$. Observations of [O I], [O II], and [O III] indicate that $\Xi \sim 10^{-3}$, implying $v_{\rm hot} \sim 300$ km s^{-1}, which is near the sound speed in the hot gas.

4.2. *The Self-Irradiated Condensing Region*

In this segment of the paper we present a model in which the cooling gas of the interfilament medium photoionizes cooled condensates. First, we consider the energetic importance of the interfilament medium and show that its luminosity can power the optical emission. Then, we present a simple model for a condensing region within an isothermal gravitational potential and show how the velocity of the flow into the condensing region determines the photoionizing flux incident upon the condensed filaments as well as their surface brightnesses.

4.2.1. *Energetics of the Interfilament Medium*

Observations of S II line ratios show that pressures within the central kiloparsec of these emission-line nebulae are 1–2×10^{-9} ergs cm^{-3} and drop off with increasing radius (HBvM; Johnstone & Fabian 1988). Presumably, the filaments are pressure-confined by hot gas at a temperature $T = T_7(10^7$ K). For the moment, let us ignore the fact that the confining gas cannot remain at this temperature without some compensating energy input. Assuming, then, that the pressure ($P = \chi n_{\rm H} kT$) at 1 kpc is P_9 (10^{-9} ergs cm^{-3}) and that the pressures vary as $r^{-\gamma}$, the luminosity of the confining gas within a radius r must be

$$L_X(<r) = (6 \times 10^{42} \text{ ergs s}^{-1})\chi^{-2} \frac{P_9^2 T_7^{-2}}{3 - 2\gamma} \left(\frac{r}{1 \text{ kpc}}\right)^{3-2\gamma} \times \frac{\Lambda}{3 \times 10^{-23} \text{ ergs cm}^3 \text{ s}^{-1}}, \tag{7}$$

if $\gamma < 3/2$. Here, Λ is the standard cooling function for a hot plasma (Raymond & Smith 1977). The spatially resolved observations of S II in Perseus by HBvM show that $\gamma < 3/2$ over the range 0–3 kpc in projected radius.

Filaments of cooler ($\sim 10^4$ K), denser gas embedded in this hot substrate can reprocess an incident soft X-ray flux into Hα radiation with a maximum efficiency of $\sim$3% (see § 5.2). If these cool clouds significantly cover the central region, the resulting Hα luminosities can approach 10^{41} ergs s^{-1} within $r \sim 1$ kpc and can exceed 10^{42} ergs s^{-1} over $r \sim 10$ kpc, depending on the value of γ. So, the radiation emerging from the confining medium can suffice to power the Hα emission regardless of how the hot gas manages to remain hot.

Rather than speculate about how the interfilament medium might be heated in situ, we will proceed under the usual assumption that as it cools and condenses, more hot gas flows inward to take its place. As we have discussed in § 4.1 and will discuss further in § 5, the spectrum radiated by gas cooling from 10^7 K through 10^5 K induces an emission line spectrum similar to that emitted by the filaments. Although we believe that a mechanism involving mass flow most naturally produces the necessary ionizing spectrum, it is conceivable that a mechanism not involving a mass flow (e.g., radio jet interactions with the interfilament medium or magnetic reconnection) might reproduce a similar ionizing spectrum, perhaps through localized episodes of heating followed by periods of cooling.

4.2.2. *Global Structure of the Condensing Region*

In Paper I, we outlined the characteristics of a central condensing region which is constantly resupplied by a cooling

flow. The hot gas in such a region will cool to filament temperatures in a time $t_c = kT/n_H\Lambda \sim (6 \times 10^6 \text{ yr}) T_7^2 P_9^{-1} \Lambda_{23}^{-1}$, where $\Lambda_{23} = \Lambda(T)/(10^{-23} \text{ ergs cm}^{-2} \text{ s}^{-1})$, and we take $\Lambda(T) \propto T^{-1/2}$. [When $T \lesssim 10^7$ K, $\Lambda(T) \approx (3 \times 10^{-23} \text{ ergs cm}^3 \text{ s}^{-1}) T_7^{-1/2}$; see Raymond & Smith 1977.] Cooling gas will flow inwards at the rate $\dot{M}_c \sim (8\ M_\odot \text{ yr}^{-1}) P_9^2 T_7^{-3} \Lambda_{23} r_1^3$, where $r_c = r_1(1 \text{ kpc})$ is the radius of the condensing region, and will release a luminosity $L_c \approx (2 \times 10^{42} \text{ ergs s}^{-1}) P_9^2 T_7^{-2} \Lambda_{23} r_1^3$. As the hot gas condenses, it fragments into clumps of column density $\gtrsim 10^{17} \text{ cm}^{-2}$, which can quickly accumulate to give a high covering factor (Paper I). Aggregates of these clouds will become gravitationally bound if their column densities exceed $\sim (7 \times 10^{22} \text{ cm}^{-2}) P_9^{1/2}$.

We can characterize the structure of a condensing region more quantitatively by solving the fluid equations for a spherically symmetric flow in which $\dot{M}$ is allowed to vary:

$$\frac{1}{r^2}\frac{d}{dr}(r^2 \rho v) = -\dot{\rho} \tag{8}$$

$$\frac{1}{\rho}\frac{dP}{dr} + \frac{GM}{r^2} = -v\frac{dv}{dr} \tag{9}$$

$$\rho v \frac{d}{dr}\left(\frac{3P}{2\rho}\right) - \frac{Pv}{\rho}\frac{d\rho}{dr} = -\left(\frac{\rho}{\bar{m}_H}\right)^2 \Lambda , \tag{10}$$

where $\rho = n_H \bar{m}_H$, v is the flow velocity, and M is the mass contained within radius r. White & Sarazin (1987a) have shown that analytical solutions to these equations can be found when the mass sink term $-\dot{\rho}$ is proportional to the density divided by the cooling time. Letting $\dot{\rho} = q(2\rho/5t_c)$, $M \propto r^\zeta$, and $\Lambda \propto T^\alpha$, they find a power-law solution in the limit of subsonic flow. In this solution, the pressure and density gradients depend on ζ and α, and the velocity gradient depends on the condensation efficiency parameter q as well. The function $\dot{M}(r)$ thus depends on the choice of q.

When the $v\,dv/dr$ term is retained, the additional constraint determines q in terms of ζ and α, and admits only one power law for $\dot{M}$. In particular,

$$n_H = n_0\left(\frac{r}{r_0}\right)^{(3/2-\alpha)(\zeta-1)-1} \tag{11}$$

$$T = T_0\left(\frac{r}{r_0}\right)^{\zeta-1} \tag{12}$$

$$v = v_0\left(\frac{r}{r_0}\right)^{(\zeta-1)/2} \tag{13}$$

$$q = \frac{5}{2}\frac{(2-\alpha)(\zeta-1)+1}{\alpha(\zeta-1)+1} , \tag{14}$$

so $\dot{M} \propto r^{(2-\alpha)(\zeta-1)+1}$. For a typical isothermal ($\zeta = 1$) potential, we then have $n_H \propto r^{-1}$, v and T constant, $\dot{M} \propto r$, and $q = 5/2$. Constraints on the power-law coefficients give the additional relations $T_0 = GMm_H/r\chi k$ and $v_0 = -r_0 n_0 \Lambda(T_0)/kT_0$. This solution is quite satisfactory for self-irradiated condensing regions because constant v implies a constant ionization parameter and $q = 5/2$ implies a condensation rate of $\dot{\rho} = \rho/t_c$.

High condensation rates such as this require the efficient growth of thermal instabilities, which are suppressed by buoyancy effects when the flow is subsonic (Loewenstein 1989; Balbus & Soker 1989). However, if q is low, the flow will accelerate as it falls into an isothermal potential (White & Sarazin 1987a, b), eventually reaching transonic velocities where q becomes high. We therefore expect v_0 to be about the sound speed at temperature T_0. Since a condensing flow into a central dominant galaxy will have

$$T_0 = (10^7 \text{ K})\frac{GM/r}{365 \text{ km s}^{-1}} , \tag{15}$$

the flow velocity in the condensing region should be several hundred kilometers per second. Velocities of this magnitude are supported by the observed characteristics of the condensing region; for $T_7 = 1$ and $\Lambda_{23} = 3$,

$$|v_0| = \frac{rP\Lambda}{\chi(kT)^2} \approx (200 \text{ km s}^{-1})\left[\frac{rP(r)}{10^{-9} \text{ kpc ergs cm}^{-3}}\right] . \tag{16}$$

4.2.3. *Photoionization of Cooled Condensates by Cooling Condensates*

As condensates drop out of the flow, they radiate $5kT/2$ per particle, generating a luminosity within radius r_0 of $4\pi r_0^2(5P_0 v_0/2)$ and giving a flux at r_0 of $5P_0 v_0/2$, equal to the flow of enthalpy into the region. By comparison, the remaining hot medium contributes a luminosity of $4\pi r_0^2 P_0 v_0$ and a flux of $P_0 v_0$, resulting from infall into the gravitational potential. Thus, radiation from the condensing gas dominates the ionizing flux, especially at EUV energies.

In the absence of cloud-cloud shielding, the spectral shape, $f(\nu)$, of this flux will be that of an ionized plasma cooling from $T_{hi} = T_7 (10^7 \text{ K})$ to $T_{lo} = 10^4$ K; hence, the expression

$$f(\nu) = \int_{T_{lo}}^{T_{hi}} \frac{\Lambda_\nu(T)}{\Lambda(T)}\,dT , \tag{17}$$

where $\Lambda_\nu(T)$ is the spectrally resolved cooling function and $\Lambda(T)$ is the total cooling function, gives $f(\nu)$ with unit normalization. Our models show that the average energy per photon emitted by gas cooling from 10^7 K is $\langle E \rangle \approx 100$ eV.

4.2.4. *Luminosity and Surface Brightness of the Condensing Region*

The Hα luminosity of the condensing region depends on three factors: the total EUV/soft X-ray luminosity emanating from the surrounding gas, the aggregate covering factor (f_c) of the filaments, and the Hα reprocessing efficiency, $\epsilon_3(0.03)$. In terms of these quantities, we then have

$$L_{H\alpha}(<r) = (3.3 \times 10^{41} \text{ ergs s}^{-1})\left(\frac{r}{1 \text{ kpc}}\right) \times \left(\frac{|v_0|}{365 \text{ km s}^{-1}}\right) P_9 f_c \epsilon_3 . \tag{18}$$

Again, we define $P_9(10^{-9} \text{ ergs cm}^{-3})$ to be the pressure at 1 kpc.

The Hα surface brightness of an individual filament will be $(5.1 \times 10^{-15} \text{ ergs cm}^{-2} \text{ s}^{-1} \text{ arcsec}^{-2})(r/1 \text{ kpc})^{-1}(|v_0|/365 \text{ km s}^{-1}) P_9 \epsilon_3$, but the observed H$\alpha$ surface brightness profile also depends on the spatial distribution of condensates, because filament superpositions will enhance the line-of-sight surface brightness. Assuming that $L_{H\alpha}$ increases smoothly like r gives the surface brightness profile

$$I_{H\alpha}(r_\perp) = (2 \times 10^{-14} \text{ ergs cm}^{-2} \text{ s}^{-1} \text{ arcsec}^{-2})\left(\frac{r_\perp}{1 \text{ kpc}}\right)^{-1} \times \left(\frac{|v_0|}{365 \text{ km s}^{-1}}\right) P_9 f_c \epsilon_3 , \tag{19}$$

when the projected radius, $r_\perp$, is substantially smaller than the radial extent of the condensing region. The average of $I_{H\alpha}$ within $r_\perp$ is $2I_{H\alpha}(r_\perp)$.

4.3. *The Photoionization Model*

The photoionization code CLOUDY (Ferland 1989), requires as input a normalized spectral shape and an intensity of incident flux. To set the incident flux we need to specify the ionization parameter and to calculate the spectral shape $f(\nu)$.

4.3.1. *Ionization Parameter*

The ionization parameter U, the ratio of the ionizing photon density and the total hydrogen density, sets the rate of energy injection per hydrogen atom into the cool filaments. For $\mathcal{F}_E = 5Pv_0/2$, $T_{fil} = 10^4$ K, $\chi = 2.4$, and $\langle E \rangle = 100$ eV,

$$U = 10^{-4.20} \frac{|v_0|}{365 \text{ km s}^{-1}} . \quad (20)$$

We test log $U = -3.90$ and -4.20, corresponding to energy fluxes of 0.207 and 0.104 ergs cm^{-2} s^{-1}, respectively, incident on cool (10^4 K) gas at a pressure of 10^{-9} ergs cm^{-3}, assuming an RS spectrum (see § 4.3.2) and $T_{hi} = 10^7$ K. Although the higher flux is difficult to generate by isothermal accretion, magnetic pressure support in the cool clouds can enhance their ionization parameter because the ambient pressure is then higher than that inferred from the S II line ratios. If β_c is the ratio of magnetic pressure to gas pressure in the cool medium, then $P/n_H = (1 + \beta_c)\chi k T_{fil}$, and the ionization parameter rises by a factor $1 + \beta_c$ (see § 6.3).

4.3.2. *Initial Temperature and Spectral Shape*

The temperature from which the ambient medium is cooling, T_{hi}, is important in determining how much energy is available to pump into the filaments and also in determining the spectral shape of the ionizing spectrum. If T_{hi} is too large, many of the ionizing photons are not absorbed efficiently because of their high energies; too low, and the total radiative energy provided is insufficient to power the filaments. For appropriate ionization parameter, we test $T_{hi} = 5 \times 10^6$, 10^7, and 2×10^7 K.

Hot gas cooling from 10^7 K through 10^5 K will emit strong EUV line radiation. To create the spectral function $f(\nu)$ we have generated broadband X-ray/EUV spectra emitted by cooling gas using an up-to-date collisional equilibrium code kindly provided by John Raymond, and we will refer to these as the RS (Raymond & Smith 1977) spectra. As an alternative input model we have also constructed an input spectrum (the GS spectrum) from several other sources: for $T = 10^{6.4}$–10^7 K we use Gaetz & Salpeter (1983) over the entire range of photon energies, and for $T = 10^5$–$10^{6.4}$ K we use Stern, Wang, & Bowyer (1978) from 13.6 to 124 eV and Raymond, Cox, & Smith (1976) above 155 eV, interpolating $f(\nu)$ linearly across the gap from 124 to 155 eV.

Although the assumption of coronal ionization equilibrium is not likely to be valid below a temperature of about $10^{6.4}$ K (Gaetz & Salpeter 1983), this is not a serious problem for two reasons. First, because the luminosity of a given layer of the cooling gas is proportional to T, the majority of the EUV spectrum is determined by the gas hotter than this temperature. Second, even though gas at cooler temperatures will be more highly ionized than it would be in equilibrium, it will still cool via emission of spectral lines in a similar band of the EUV spectrum. Nevertheless, an accurate treatment of the nonionizing C IV, N V, and O VI emission from these flows will require a nonequilibrium calculation.

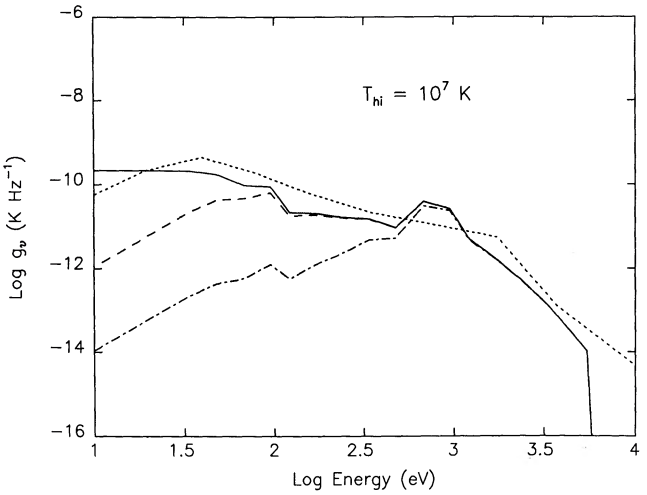

FIG. 1.—Raymond-Smith (RS) and Gaetz-Salpeter (GS) input spectra [$g_\nu \equiv T_{hi} f(\nu)$] for $T_{hi} = 10^7$ K. The solid line is the RS spectrum, the dotted line is the GS, the dashed line is RS plus 10^{19} cm^{-2} of cloud shielding as described in § 5.6, and the dash-dot line is RS plus 10^{21} cm^{-2} of cloud shielding. Note that the RS spectrum is softer in the 100–200 eV range, but has relatively more emission at 1 keV.

In Figure 1, we compare the two spectral models for emission from plasma cooling from $T_{hi} = 10^7$ K. The RS model is somewhat softer than the GS model in the 100–200 eV band, but has a large contribution at ~ 1 keV from Fe L-shell line emission. These differences are due to discrepancies in the assumed oscillator strengths, particularly those of emission lines from the middle ionization states of iron. The RS code we use is more recently revised than the GS model, but some of the atomic data used in both models may be inaccurate, so it is unclear which model is superior.

5. RESULTS

Using the photoionization code CLOUDY (Ferland 1989), we have calculated the optical emission-line spectra induced in a cool ($\sim 10^4$ K) filament by the ionizing flux specified by the ionization parameter, U, and total hydrogen density, n_H, at the cloud boundary, and the initial temperature T_{hi}. The cloud is assumed to be of cosmic abundances and in pressure equilibrium. We investigated how differing hydrogen column densities affect the resulting line ratios, but we were limited at the high column density end because CLOUDY can assume only trace amounts of molecular hydrogen.

5.1. *Standard Model*

Our "standard" model has log $U = -3.90$, $T_{hi} = 10^7$ K, and $n_H = 300$ cm^{-3}. In Figures 2 through 7, we plot with solid lines the line ratios characteristic of these parameters for hydrogen column densities (N_H) ranging from $10^{17.5}$ to 10^{22} cm^{-2}, along with data from HBvM. The tick marks along the lines in the plots represent $N_H = 10^{17.5}$, 10^{18}, 10^{19}, $10^{19.3}$, $10^{19.5}$, $10^{19.7}$, 10^{20}, 10^{21}, $10^{21.5}$, and 10^{22} cm^{-2}. Here, variations in the column densities of the individual filaments adequately reproduce the range of line ratios in cooling flow filaments. The "class I" filaments appear to have total hydrogen column densities of $10^{17.5-18.5}$ cm^{-2}, and the "class II" filaments are well modeled by clouds of $10^{20.5-22}$ cm^{-2}. The gap at $10^{18.5-20.5}$ cm^{-2} may be due to the lack of data for

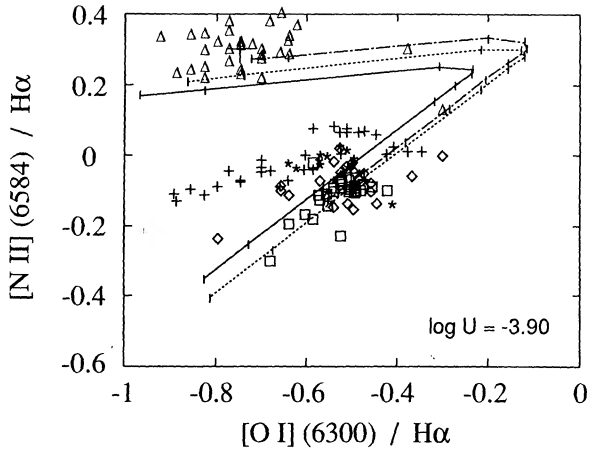

FIG. 2.—[O I] (λ6300)/Hα vs. [N II] (λ6584)/Hα for ionization parameter log $U = -3.90$. The solid line is for $T_{hi} = 10^7$ K, the dotted line is for $T_{hi} = 2 \times 10^7$ K, and both of these lines are for the RS spectrum. The dash-dot line is for a GS spectrum with $T_{hi} = 10^7$ K. Column densities (log N_H in cm^{-2}) range from 17.5 to 22.0. The low column density models are at the top of the plot, the high column density models are at the lower left-hand corner of the plot, and the tick marks indicate log N_H of 17.5, 18, 19, 19.3, 19.5, 19.7, 20, 21, 21.5, and 22. Average line ratios for "class I" and "class II" objects are represented with large crosses. Line points (kindly provided by S. Baum) of triangles represent M87 = Virgo, small crosses are NGC 1275 = Perseus, asterisks are PKS 0745−191, x's are 3C 317 = A2052, diamonds are A1795, and squares are PKS 2322−122 = A2597.

many different clusters, or it may be due to fundamental differences in the filaments' structure (see § 6.1).

5.2. *Column Density Dependence*

When we vary the column density in our models, we find that we can reproduce the range of line ratios observed in HBvM. The low column density models ($N_H \sim 10^{17.5-18.5}$ cm^{-1}) give [N II]/Hα ratios of ~2, as observed in class I filaments. At the other extreme, high column density models ($N_H \sim 10^{20.5-22}$) give [N II]/Hα ratios of ~1, as observed in class II filaments. The [N II]/Hα ratios can be understood as a heating-per-ionization diagnostic. If EUV (~100 eV) photons are ionizing a highly ionized plasma, they deposit 80%–90% of their energy as heat (the rest goes towards photoionization.) Since [N II] is collisionally excited by thermal electrons, this line measures the heating rate in the gas, whereas the Hα line

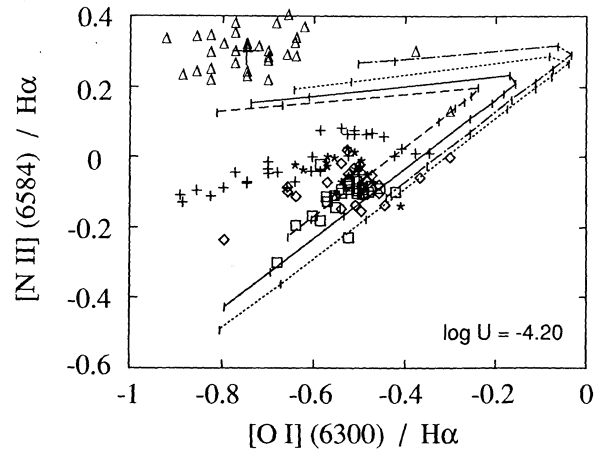

FIG. 3.—[O I] (λ6300)/Hα vs. [N II] (λ6584)/Hα for ionization parameter log $U = -4.20$. The key is the same as for Fig. 2, except in that the dashed line is for an RS spectrum with $T_{hi} = 5 \times 10^6$ K.

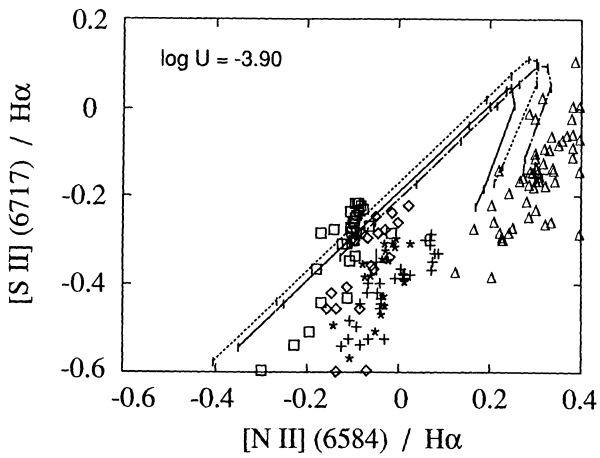

FIG. 4.—[N II] (λ6584)/Hα vs. [S II] (λ6716)/Hα for log $U = -3.90$. The symbols and lines are the same as in Fig. 2. The low column densities start at the central right portion of the plot, and the high column densities are at the lower central portion of the plot.

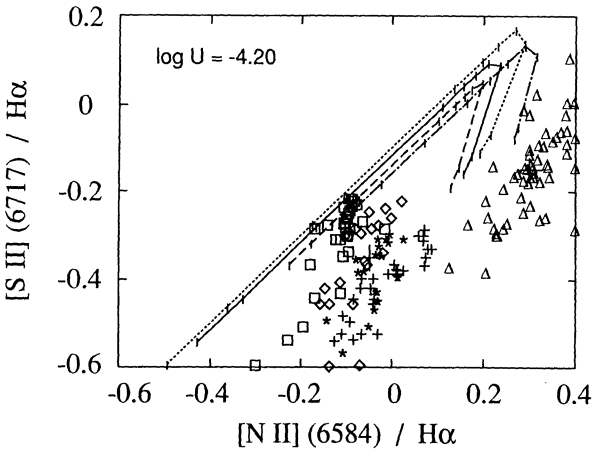

FIG. 5.—[N II] (λ6584)/Hα vs. [S II] (λ6716)/Hα for log $U = -4.20$. The symbols and lines are the same as in Fig. 3. The low column densities start at the central right portion of the plot, and the high column densities are at the lower central portion of the plot.

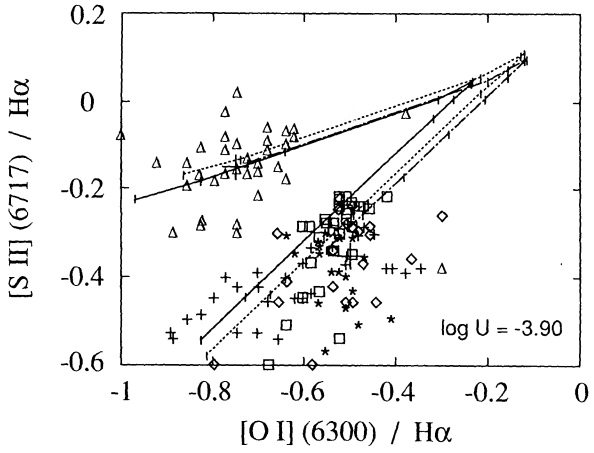

FIG. 6.—[O I] (λ6300)/Hα vs. [S II] (λ6716)/Hα for log $U = -3.90$. The symbols and lines are the same as in Fig. 2. The low column densities are at the central left-hand portion of the plot, and the high column densities are at the low central portion of the plot.

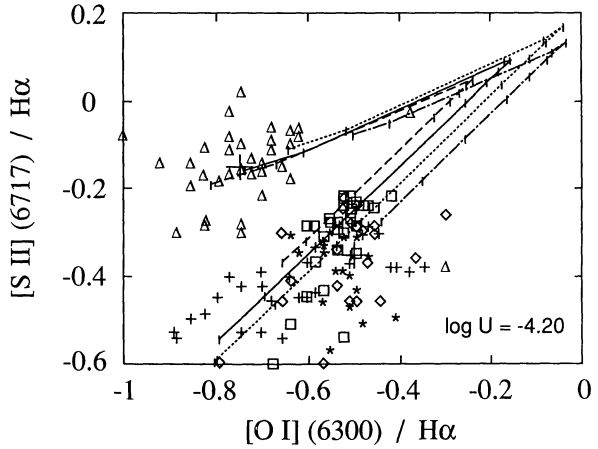

FIG. 7.—[O I] (λ6300)/Hα vs. [S II] (λ6716)/Hα for log $U = -4.20$. The symbols and lines are the same as in Fig. 3. The low column densities are at the central left-hand portion of the plot, and the high column densities are at the low central portion of the plot.

measures the ionization rate. The large amount of heating per ionization leads to the large [N II]/Hα and [O II]/Hα ratios. However, as the column density of the gas increases, the ionization fraction of the gas decreases and higher energy photons are absorbed, producing X-ray photoelectrons which not only heat the gas but also collisionally ionize hydrogen. This results in more Hα and reduces the [N II]/Hα ratio to ~ 1.

Variations in column density also produce variations in the [O I]/Hα and [S II]/Hα ratios. These line ratios indicate the presence of a partially ionized region, photoionized by EUV and soft X-ray photons. Initially, as the column density increases, [S II] and [O I] increase relative to Hα because the volume of the warm, partially ionized region containing these species also increases. At higher column densities, the electron temperature becomes too low to excite these lines, and the [O I] and [S II] emission remain constant while ionizations continue to produce Hα, lowering the [O I]/Hα and [S II]/Hα ratios.

We plot the Hα conversion efficiencies in Figure 8 for various input spectra. Note that these efficiencies are for individual cloudlets; the overall efficiency of a collection of thin filaments would approach that of a single thick filament. An individual cloudlet of specified column density will convert the incident spectral flux, determined by T_{hi}, U, and n_H, to Hα radiation with an efficiency of not more than 3% (i.e., 3% of the incident luminosity is re-emitted in the Hα line.) For low column density filaments ($\sim 10^{17.5}$ cm^2) the efficiency is a factor of 10 lower due to the penetration and escape of the high-energy photons. However, if many low column-density filaments lie along a typical line-of-sight, the Hα reprocessing efficiency would be higher, $\sim 1\%$ for a total column density of 10^{19} cm^{-2}.

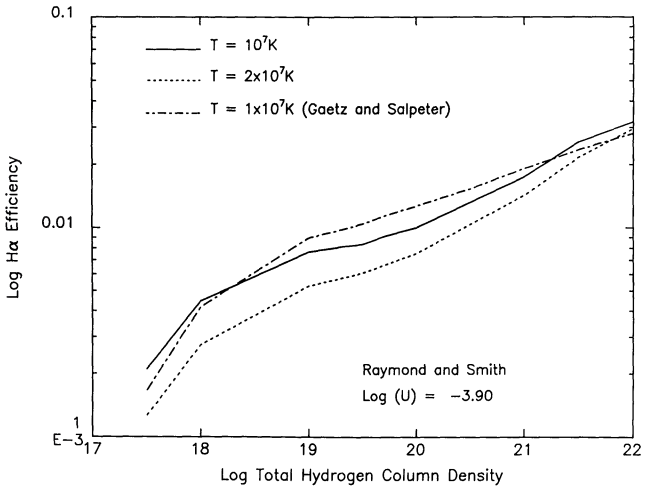

FIG. 8.—Hα convesion efficiencies for various input spectra vs. cloudlet column density. The vertical axis gives the fraction of the incident flux that re-emerges in the Hα line. The RS spectra are used unless otherwise indicated.

5.3. *Variations in T_{hi}*

The lower T_{hi}, the easier it is to convert cooling radiation to Hα emission. This is due to the predominance of soft photons in the spectrum of a plasma cooling from lower temperatures. Soft photons are more easily trapped, so a higher fraction of the photons from a cooler plasma are absorbed by a thin filament. Nevertheless, the efficiency of conversion to Hα still never exceeds $\sim 3\%$.

When we vary T_{hi} and hold the ionization parameter and total hydrogen density constant at the boundary of the filaments, the emission-line ratios change as shown in our Figures 2, 4, and 6. The hotter T_{hi}, the more [S II] and [O I] are produced per Hα photon. For class I filaments, more [N II] is produced. At higher column densities and higher T_{hi}, X-ray photoionization becomes increasingly more important, leading to more high-energy photoelectrons and more nonthermally excited Hα emission.

5.4. *Other Parameter Variations: Ionization Parameter and Spectral Model*

When we vary the ionization parameter, we change the emission ratios of [O I]:[O II]:[O III] as well as [S II]:[S III] because we are changing the ionization state of the gas. Values of log U from -3.90 to -4.20 seem to adequately straddle the range of line ratios observed. If U is higher, too much [O III] is produced. If U is lower, the [O I]/Hα and [S II]/Hα line ratios become higher than observed.

A comparison of the line ratios generated by the two different types of input spectra, RS and GS, shows some differences. We find that the RS models have lower [N II]/Hα ratios because of the relative lack of 100 eV photons and also result in a lower production of [O I]. In the low column density models with RS spectra, [N II]/Hα is slightly lower than the observed values when $T_{hi} \lesssim 2 \times 10^7$ K, but cloud-cloud shielding might also be important here (see § 5.6). The GS models tend to overproduce [O I] with respect to Hα, because the relative EUV hardness of the GS spectrum enlarges the region in which warm, neutral oxygen exists. However, the prominent iron L-shell lines in the RS spectrum give a larger amount of nonthermal Hα emission deeper within the cloud.

Both types of input spectrum give roughly the same conversion efficiencies, although the GS input spectrum is converted approximately 30% more efficiently at total hydrogen column densities of 10^{19} cm^{-2}. Both the RS and GS spectra give a maximum Hα conversion efficiency $\sim 3\%$ at column densities $\gtrsim 10^{22}$ cm^{-2}.

5.5. *Other Spectral Diagnostics*

Infrared S III (λλ9526, 9096) lines have been touted as a possible diagnostic to distinguish between shocks and photo-

ionization, with photoionization giving higher [S III]/Hα ratios (Diaz, Pagel, & Wilson 1985; Diaz, Pagel, & Terlevich 1985). However, high-velocity shocks (Binette et al. 1985) can boost [S III] emission, and in our photoionization models, we can obtain low [S III]/Hα ratios by lowering the column densities of the individual filaments or by lowering the ionization parameter. Thus, [S III] observations might not be a critical test for shocks or photoionization.

Because some of the higher ionization lines in the optical and ultraviolet are created in the nonequilibrium cooling stage of a forming condensation (Binette et al. 1985), we are refraining from publishing a complete table of line ratios with this paper. Work is in progress on a model which includes both the nonequilibrium cooling and photoionization contributions to the line emission.

5.6. *Cloud-Cloud Shielding*

When cloudlets are sufficiently numerous to begin shielding each other from the radiation bath of the cooling gas, the spectra seen by the individual clouds differs from the generic cooling spectra we have been assuming. To study this effect, we have generated a model in which thin ($\lesssim 10^{18}$ cm^{-2}) filaments are distributed evenly throughout the condensing region so that any line of sight through the region intercepts 10^{19} cm^{-2} of filament material. The effect of shielding in such a system will be to attenuate the incident spectrum by a factor of roughly $(1 - e^{-\tau})/\tau$, where τ is the optical depth of a 10^{19} cm^{-2} cloud of cool gas at the frequency of interest. (See Fig. 1 for input spectra.)

The soft photons below $E \sim 3$–4 Rydbergs are effectively removed by neutral hydrogen and helium photoabsorption, so the effective ionization parameter of these models is low. However, we keep the 400 keV flux the same in the shielded and unshielded models in order to isolate the effects of attenuation. We find that the attenuated input spectrum boosts [N II]/Hα considerably and somewhat boosts [O I]/Hα. Inhomogeneities in the distribution of filaments would result in an input spectrum combining attenuated and unattenuated spectra, with perhaps some contribution from starlight in regions particularly well-shielded from the ambient EUV flux. Since we have no a priori specification of filament structure, we did not model more complicated shielding geometries.

6. DISCUSSION

Our simple model for self-irradiated cooling condensations predicts emission-line ratios very similar to those observed, and we reproduce the observed range of line ratios by varying a single parameter, the cloudlet column density. This mechanism predicts a high efficiency for converting the incident EUV and soft X-ray photons into optical line emission, sufficient to explain the high luminosities of the optical emission lines (Paper I). The ionization parameter and surface brightness of a condensing region are set by the inflow velocity, and its boundary is essentially the sonic radius of the cooling flow. If the optical emission lines in clusters come from self-irradiated condensing regions of the kind described here, the implications for cooling flows are far-reaching.

6.1. *Class I versus Class II*

The line ratios of the optical filaments at the centers of cooling-flow clusters tend to fall into a bimodal distribution when plotted on line ratio diagrams (HBvM; see Figs. 2–7). Our photoionization models show that the differences between class I and class II line ratios can be interpreted as a difference in the column densities of the irradiated cloudlets. Class I line ratios arise in 10^{17-18} cm^{-2} cloudlets, whereas class II line ratios indicate much thicker 10^{21-22} cm^{-2} clouds. Although the gap at intermediate column densities ($10^{18.5-20.5}$ cm^{-2}) appears to be real, the data remain sparse. The high Hα luminosities of class II clusters support this interpretation. For a given X-ray derived $\dot{M}$, class II clusters tend to be significantly brighter in Hα than class I clusters (HBvM), and these higher Hα outputs should be expected if the more efficient high column-density clouds populate class II clusters.

This dichotomy, if it proves to be real, could be rooted in the difference between self-gravitating and fragmented clouds. As a condensation forms, hydrodynamic instabilities will tend to tear it apart (see Nulsen 1986). These instabilities will work to maintain the cloud in a fragmented state wherein the fragments have a thickness of order the cooling time times the sound speed, corresponding to a column density $\sim 10^{17}$ cm^{-2} in gas that has recently cooled through 10^5 K (Paper I). The accumulating fragments will coalesce when their self-gravity suffices to bind them. Gravitational binding of 10^4 K gas at these densities requires a column density $\gtrsim 10^{22}$ cm^{-2}. Recent observations of a star-forming region within a filament in NGC 1275 (Shields & Filippenko 1990), a class II cluster, imply that at least some of this gas has become gravitationally bound. Given this scenario, it is possible that both types of filament class may exist in a single cluster, because some filaments may have coalesced, while others remain fragmented. In fact, line ratios from a single galaxy which fall into both classes may have been seen in some filament systems already (Fabian 1990, private communication).

6.2. *Flow Velocity*

In the type of condensing region described in § 4, both the ionization parameter and the surface brightness profile are determined by the inflow velocity. The overall luminosity of the region depends on the inflow velocity and the region's radius. When only thermal energies and pressures are considered, an inflow velocity of 365 km s^{-1}, equal to the isothermal sound speed at 10^7 K, gives $\log U = -4.20$, on the low end of acceptable ionization parameters. This same velocity gives an Hα surface brightness profile $I_{\mathrm{H}\alpha}(r_\perp) = (2 \times 10^{-13}$ ergs cm^{-2} s^{-1} arcsec$^{-2})(r_\perp/1$ kpc$)^{-1} P_9 f_c \epsilon_3$ and a luminosity of $(3.3 \times 10^{41}$ ergs s$^{-1})(r_{\mathrm{H}\alpha}/1$ kpc$) P_9 f_c \epsilon_3$, where $r_{\mathrm{H}\alpha}$ is the radial extent of the Hα emission region.

Detailed brightness profiles of PKS 0745−191 and A2597 obtained by HBvM show that $I_{\mathrm{H}\alpha}$ falls off like $r_\perp^{-1}$ out to 5–7 kpc and more quickly thereafter. The total Hα luminosities of these objects, taken to be 0.5 times the Hα + [N II] luminosities, are both 1.4×10^{42} ergs s^{-1}. These values are consistent with a condensing region ~ 10 kpc in radius having an inflow velocity of a few hundred kilometers per second, a covering factor slightly less than unity, and a 3% Hα reprocessing efficiency. Hu et al. (1985) measured the central Hα + [N II] surface brightnesses in several clusters of galaxies, typically finding a brightness of several times 10^{-15} ergs cm^{-2} s^{-1} arcsec^{-2} within the central kiloparsec or so, also consistent with the above picture. NGC 1275 in Perseus, an exceptional case, we will discuss in depth below (§ 6.5).

Observations of emission-line widths also support the condensing region hypothesis. The velocity widths (FWHM) measured by HBVM tend to run from ~ 200 km s^{-1} at projected radii of 10 kpc to $\gtrsim 600$ km s^{-1} near zero projected radius,

with a typical value ~ 300 km s^{-1} and a large dispersion. In a constant-velocity condensing region, the radial gradient would arise because cloudlets at small projected radii would be travelling more directly along the line of sight. A more comprehensive model of the spatial distribution of condensates is necessary before detailed line profiles can be computed.

6.3. *Other Sources of Internal Energy*

An ionization parameter of $\log U = -3.90$ gives the most convincing agreement between our photoionization model for unshielded clouds and the observed line ratios, but it implies an uncomfortably large inflow velocity (~ 700 km s^{-1}). More sophisticated models for the input spectra incorporating newer atomic data and cloud-cloud shielding effects may eventually give better agreement for lower velocity flows. However, it is also possible that nonthermal sources of internal energy such as magnetic fields (Tribble 1991) or turbulence (Loewenstein & Fabian 1990) modify our simple $5kT/2$ prescription for the internal energy per particle and our assumption of purely thermal pressure support, changing the relation between inflow velocity and ionization parameter.

6.3.1. *Magnetic Energy*

Rotation measure observations provide ample evidence of magnetic fields in cooling flows. Radio emission has been associated with cooling-flow clusters having optical line emission (e.g., Burns 1990; Jones & Forman 1984; O'Dea & Baum 1987; Baum & Heckman 1990), while rotation measure observations of Cygnus A (Dreher, Carilli, & Perley 1987), M87/Virgo and A1795 (Owen et al. 1989) and 3C 295 (Kato et al. 1987) also indicate the presence of sizeable magnetic fields. Soker & Sarazin (1990) show these magnetic fields can come into equipartition with the thermal pressure within radii of ~ 10 kpc. Condensations developing in this kind of magnetized medium must dissipate their magnetic support, remaining close to equipartition while they collapse.

We can construct a correction factor for the ionization parameter by parameterizing the various forms of internal energy and pressure support available in a condensing region. Let $P_c = \chi n_{\rm H} kT$ be the gas pressure of the optically emitting clouds and β_c be the ratio of magnetic pressure to gas pressure in this cool gas. Similarly, let P_h and $\beta_h P_h$ be the gas and magnetic pressures in the hot gas. In addition, suppose that other sources of internal energy in the hot gas contribute a pressure $\beta_o P_h$ and an energy density $\epsilon_o \beta_o P_h$. Assuming that condensations dissipate their non-thermal internal energy into heat as they cool, the ionization parameter of the condensates then becomes

$$U = 10^{-4.20}\left(\frac{|v_0|}{365 \text{ km s}^{-1}}\right)\mathscr{I}\,, \tag{21}$$

where

$$\mathscr{I} = \frac{2}{5}\left[\frac{(5/2) + \beta_h + \epsilon_o\beta_o}{1 + \beta_h + \beta_o}\right](1 + \beta_c)\,. \tag{22}$$

Amplification of the ionization parameter thus occurs most readily when magnetic pressure is important in the clouds but not in the hot medium. Other sources of internal energy can increase the ionization parameter only if their characteristic ratio of internal energy to pressure, ϵ_o, is greater than 5/2. If the emission-line clouds really are self-irradiated cooling condensations, more sophisticated photoionization models might allow us to assess the role of magnetic pressure support through line-ratio studies.

6.3.2. *Turbulent Mixing Layers*

If turbulence is important in cooling flows, "turbulent mixing layers" of the type proposed by Begelman & Fabian (1990) can arise and power an optical emission-line spectrum. These models, in which the hot gas mixes with the cooler clouds creating an EUV-emitting mixing layer, are similar to ours, except the characteristic temperature of the irradiating gas is $\sim 10^{5.5}$ K, compared to 10^{6-7} K in our models. [A general result of adiabatic mixing is that the temperature of the mixed material becomes $T_f \sim (T_{\rm hot}\, T_{\rm cool})^{0.5}$.] Since the characteristic photon energy of the incident spectrum is lower, the [N II]/Hα ratio (a heating/ionization diagnostic; see § 5.2) tends to be too low to explain the range of [N II]/Hα ratios seen in cooling flows. Also, such mixing layers should be emitting a prodigious luminosity in the O VI and/or C IV lines. The emission-line widths in these models, rather than being generated by infall, are explained by turbulence.

The radiation from this mixing layer is efficiently absorbed by low column density filaments, because of the low characteristic energy of the photons in the incident spectrum. However, the efficiency of converting incident radiation into Hα will never exceed $\sim 3\%$. Pure case B hydrogen recombination gives an Hα efficiency of only $\sim 6\%$, while optical forbidden lines radiate another large portion of the incident luminosity. If the ultimate source of energy is the cooling flow itself, the relationship between $\dot{M}(r)$ and $L_{\rm H\alpha}(<r)$ in the turbulent mixing layer model must therefore be similar to that in a cooling condensation model.

6.4. *Determining $\dot{M}$*

One possible benefit of studying the optical emission lines in cooling flows is to determine $\dot{M}$ in their central regions, which are unresolvable with present X-ray telescopes. One must also ask whether the values of $\dot{M}$ derived from the optical lines are consistent with those derived from the X-ray data. Before $\dot{M}$ can be estimated from $L_{\rm H\alpha}$, the total column density and covering factor of the filaments must be known so that a conversion efficiency can be calculated. Although the column densities of individual cloudlets can be estimated from the observed line ratios, it remains unclear how many such cloudlets lie along a given line of sight. Eventually, detailed spatial and spectral observations of soft X-ray absorption in the Hα-emitting region might yield these values.

Our photoionization models show that class II clusters, at least, appear to contain thick filaments, so we can derive a useful lower limit on the $\dot{M}$ responsible for the Hα emission by assuming 3% conversion efficiency, $T_{\rm hi} = 10^7$, and a high covering factor; specifically,

$$\dot{M}_{\rm H\alpha} = (16\ M_\odot\ \text{yr}^{-1})\left(\frac{L_{\rm H\alpha}}{10^{41}\ \text{ergs s}^{-1}}\right)(T_7 f_c \epsilon_3)^{-1}\,. \tag{23}$$

In Paper I, we showed that for the clusters studied by HBvM, $\dot{M}_{\rm H\alpha}$ is less than or equal to the X-ray derived $\dot{M}$, in most cases lower by a factor of more than 10. The cooling condensation model therefore does not overdraw the overall mass/energy budget of the cooling flow, as do some of the models mentioned in § 3.

Within the condensing region itself, $\dot{M}(r)$ should be proportional to r. In a cluster with $L_{\rm H\alpha} = 1.4 \times 10^{42}$ ergs s^{-1} distributed over the central 10 kpc (see § 6.2), the required

$\dot{M}_{H\alpha}(r)$ is $(22\ M_\odot\ \mathrm{yr}^{-1})(r/1\ \mathrm{kpc})\ (T_7 f_c \epsilon_3)^{-1}$. According to our model for the condensing region, the mass flow determined by the inflow velocity v_0 and the pressure $P_9(10^{-9}$ ergs $\mathrm{s}^{-1})$ at $r = 1$ kpc is

$$\dot{M} = (30\ M_\odot\ \mathrm{yr}^{-1})\left(\frac{r}{1\ \mathrm{kpc}}\right)\left(\frac{|v_0|}{365\ \mathrm{km\ s}^{-1}}\right)P_9\ , \qquad (24)$$

where $T_7 = 1$. This agrees well with the required value, considering the underlying uncertainties.

These high mass flow rates at small r appear to conflict with studies of X-ray surface brightness profiles that suggest $\dot{M}(r)/r \sim 1\ M_\odot\ \mathrm{yr}^{-1}\ \mathrm{kpc}^{-1}$ (Thomas et al. 1987; White & Sarazin 1988). In fact, the apparent conflict might indicate a fundamental difference between various kinds of cooling flows. The set of flows studied by both Thomas et al. (1987) and HBvM contains eight members: A85, A626, A496, Centaurus, MKW 3s, A2063, A2199, and Cygnus A. We delete Cygnus A from this sample because its Hα emission is likely to be powered by an AGN (HBvM). All of the remaining seven have Hα luminosities giving a required $\dot{M}$ less than 10% of the X-ray derived value. Perhaps low, sometimes unobservable Hα luminosities occur when mass is deposited at large radii, while high Hα luminosities occur when much of the mass reaches the center. Paper I speculates that differences in mass deposition rates might reflect differing degrees of homogeneity in the flows. We mention one caveat here and discuss it further in § 6.5: soft X-ray absorption by thick clouds at the centers of cooling flows might mimic the central surface-brightness flattening used to model the mass deposition profiles.

If large mass flows do indeed reach the centers of some clusters, what is the dynamical fate of the deposited material? Velocity-dispersion arguments are sometimes employed to constrain the timescale over which a flow of this magnitude can persist (e.g., Hu et al. 1985). The contribution to the cluster potential due to accreted material is taken to be $G\dot{M}(r)/r$ times the lifetime of the flow. For $\dot{M}(r)/r \sim 10\ M_\odot\ \mathrm{yr}^{-1}\ \mathrm{kpc}^{-1}$, the implied velocity dispersion will exceed a couple hundred km s^{-1} in a tenth of a Hubble time, apparently constraining such flows to be shortlived. Such clusters, in which $\dot{M}_{H\alpha}$ is close to the X-ray derived $\dot{M}$, do represent only a small minority of all cooling-flow clusters (see Paper I).

However, a simple estimate like this fails to account for the kinetic energy of the condensates at the time they decouple from the flow. Self-gravitating knots of gas that decouple from the flow and become collisionless will have an initial velocity equal to the flow velocity at the point of decoupling. If the velocity of such a knot is somewhat higher than the average stellar velocity in the central galaxy, the dynamical relaxation of the knot will tend to *decrease* the overall velocity dispersion of the galaxy. Conversely, collisionless knots that are initially slow-moving will tend to *increase* the velocity dispersion of the galaxy. It is therefore unclear how a high $\dot{M}$ flow which enters a central condensing region at several hundred km s^{-1} will affect the central velocity dispersion of the underlying galaxy. A dynamical investigation is needed to determine how this process works in detail.

6.5. *Perseus: A Special Case?*

The spectacular, unusually extended ($\sim$100 kpc) filament system in Perseus/NGC 1275/A426 is considered the archetypal example of Hα emission from a cooling flow; however, the Seyfert nucleus at its core complicates the analysis of its Hα and X-ray emitting processes. This cluster has a huge Hα luminosity ($2.1 \times 10^{42} h_{75}^{-2}$ ergs s^{-1}, where $h_{75} = H_0/75$ km s^{-1}), plus a central X-ray point source emitting $\sim 7 \times 10^{43} h_{75}^{-2}$ ergs s^{-1} (Branduardi-Raymont et al. 1981). Mass accretion rates into NGC 1275 have been derived by several workers: White & Sarazin (1988) find rates of 300–500 $M_\odot\ \mathrm{yr}^{-1}$, with a decrease of $\lesssim$40% from 200 kpc to 20 kpc, while Fabian et al. (1984) report a steeper radial variation of 250–20 $M_\odot\ \mathrm{yr}^{-1}$ from 150 to 20″, equivalent to $53 h_{75}^{-1}$ to $7 h_{75}^{-1}$ kpc for $z = 0.0183$. To evaluate observationally whether there is enough energy emitted by the cooling gas in Perseus to power the filaments, i.e., whether the surface brightness in X-rays is comparable to the surface brightness in optical lines, is a difficult task, owing to the uncertainties in removing the effects of the central point source. We have taken a closer look at Perseus in order to determine whether the scenario we propose in this paper can be applied here.

6.5.1. *A Direct Surface Brightness Comparison*

If the X-ray emission in the central portion of the cluster comes from the same cooling gas whose X-ray and EUV emissions power the optical lines, then the ratio of the co-extensive X-ray flux (F_X) to $F_{H\alpha+[N\ II]}$ should be $\gtrsim (2 \times 0.03)^{-1} \approx 17$ (Meiksin & Davis 1989, private communication, cited in HBvM), presuming that less than half the X-ray energy is absorbed. HBvM show that this condition is satisfied in M87, A496, PKS 0745−191, and, without accounting for the point-source contribution, NGC 1275. Here, we make a more precise comparison using Hα + [N II] surface brightness data from Heckman (1981) and X-ray surface brightness data from the HRI observations of Branduardi-Raymont et al. (1981). We correct the Hα + [N II] fluxes for galactic reddening by a column of 1.6×10^{21} cm^{-2} to Perseus (Gorenstein et al. 1978), assuming a dust optical depth at λ6563 of $\tau_{ext} = (0.4 \times 10^{-21}) N_H^{gal}$, where N_H^{gal} is the total galactic hydrogen column density in cm^{-2} (Draine & Lee 1984; Savage & Mathis 1979).

Branduardi-Raymont et al. (1981) use the HRI surface brightness profile of NGC 1275 to separate the point-source (AGN) and extended (cooling-flow) contributions to the overall X-ray flux. After the point source is subtracted, the remaining flux fits the profile

$$F_X(<r_\perp) = (2.1 \times 10^{-10}\ \mathrm{ergs\ cm}^{-2}\ \mathrm{s}^{-1}) \times \ln\left[1 + \left(\frac{r_\perp h_{75}}{26\ \mathrm{kpc}}\right)^2\right], \qquad (25)$$

assuming a 1 keV bremsstrahlung spectrum obscured by the same hydrogen column density we used in the reddening correction. Because of the point-spread function, the point source greatly dominates the extended emission within $r_\perp \approx (7\ \mathrm{kpc}) h_{75}^{-1}$, where the point-source subtracted profile becomes less reliable.

Using this extrapolated profile, we have compared the X-ray and Hα fluxes within radii of 7″, 14″, 28″, and 75″, corresponding to $r_\perp$ of 2.5, 5.0, 10.0, and 27 in units of h_{75}^{-1} kpc. The upper portion of Table 1 gives the flux ratios when the X-ray point source is included, and the resulting ratios all healthily exceed the limiting value. The lower portion of the table gives the flux ratios when the X-ray point source is excluded and the Hα + [N II] from the central 7″, which might be generated by the AGN, is subtracted. These ratios are unfavorable, but when the extended X-ray flux is taken to have a shape characteristic

TABLE 1

NGC 1275 SURFACE BRIGHTNESS DATA

Θ (1)	$F_{H\alpha+[N\,II]}(<\Theta)$ (2)	$F_X(<\Theta)$ (3)	Ratio (4)
7.....	2.70	84	31.1 (67.0)
14.....	4.05	89	22.0 (47.3)
28.....	5.40	110	20.4 (43.9)
75.....	13.9	230	16.4 (35.3)
7.....	...	1.84	...
14.....	1.35	7.24	5.4 (11.6)
28.....	2.70	27.6	10.2 (21.9)
75.....	11.2	146	13.0 (28.0)

NOTES.—Col. (1) Radius in arcsec (Scale = 0.355 arcsec^{-1} kpc h_{75}^{-1}); Col. (2) Hα + [N II] flux within the specified radius in units of 10^{-12} ergs cm^{-2} s^{-1}, corrected for Galactic extinction (Heckman 1981; HBvM); Col. (3) Total (bolometric) X-ray flux in units of 10^{-12} ergs cm^{-2} s^{-1}, assuming 1 keV bremsstrahlung and $N_H = 1.6 \times 10^{21}$ cm^{-2} of absorbing column density (Branduardi-Raymont et al. 1981); Col. (4) Ratio of F_X and $F_{H\alpha+[N\,II]}$. In parentheses is the ratio assuming F_X is emitted from cooling condensates (assuming Gaetz and Salpeter spectrum). In the second half of the table, we have subtracted the Hα emission interior to 7″ and the X-ray point-source contribution in order to account for radiation possibly associated with the Seyfert nucleus.

of cooling condensations, rather than of 1 keV bremsstrahlung, the agreement becomes marginal. Obviously, we must evaluate the role of the point source in generating Hα emission.

6.5.2. *The AGNs Zone of Influence*

Although HBvM and Johnstone & Fabian (1988) have convincingly shown that the AGN cannot be creating the entire photoionized nebula in NGC 1275, the AGN may still be exciting some circumnuclear Hα. An AGN's "zone of influence" will end at the radius, r_{AGN}, where the ambient photoionizing flux begins to exceed that from the AGN. The Branduardi-Raymont et al. (1981) observations suggest that the extended flux does not exceed the point-source flux until $r_\perp > (18\ \mathrm{kpc})h_{75}^{-1}$, far too large to agree with the emission-line ratio maps.

Alternatively, we can address this question from the viewpoint of a condensing-region model. Equating the energy flux $5Pv_0/2$ to the AGN flux gives

$$r_{AGN} = (2.5\ \mathrm{kpc})h_{75}^{-1}P_9^{-1/2}\left(\frac{|v_0|}{365\ \mathrm{km\ s^{-1}}}\right)^{-1/2}, \quad (26)$$

corresponding to a projected radius about half this size, within which the ionization parameter will begin to vary like r^{-1}, as long as $P(r)$ remains proportional to r^{-1}. Two pieces of observational evidence hint at a possible qualitative change in the nebula at close to this radius. First, the Hα + [N II] surface brightness profile given by HBvM begins to rise abruptly within $r_\perp = (1\ \mathrm{kpc})h_{75}^{-1}$ and peaks at a level several times higher than any other measured cluster (Hu et al. 1985). Outside this radius and out to 10 kpc the brightness profile is quite similar to the others measured by HBvM. Second, certain line ratios measured by Johnstone & Fabian (1988) vary anomalously within ~2 kpc. In particular, [O I]/(Hα + [N II]), everywhere else constant within 30%, rises by a factor of 2, to a value more in accord with AGN photoionization. However, without more complete spatial and spectral data, it is unclear what this rise really means.

6.5.3. *Soft X-Ray Covering*

If the AGN's zone of influence is this small, then much of the soft X-ray cooling radiation from the condensing region is not seen by *Einstein*. White & Sarazin (1988) encountered a similar problem in trying to determine $\dot{M}(r)$ in NGC 1275 from the same data. They found that ~300 $M_\odot$ yr^{-1} appeared to be entering the central 20 kpc, but that only ~20% of the expected luminosity then emerged from that region. We propose that the same thick clouds responsible for the optical emission also obscure the X-ray flux from the center of this cluster.

Clouds of column density $\sim 10^{22}$ cm^{-2} will be optically thick to 1 keV photons but marginally transparent to 2 keV photons and will absorb the large majority of the radiation from 10^7 K cooling condensations while transmitting some of the harder AGN continuum. Combining $\dot{M} = 300\ M_\odot$ yr^{-1}, $v = 300$ km s^{-1}, and $r = 10$ kpc gives 10^{22} cm^{-2} as a crude dimensional estimate for the mean obscuring column density in condensates. Since these clouds will have formed out of dust-free intracluster gas (Fabian, Nulsen, & Canizares 1982), their optical extinction should be negligible. If the cooling-condensation model is correct, the energetics of this source *require* a covering factor of high column density clouds near unity (Paper 1), making it *necessary* that there be some significant dimming of the central X-ray surface brightness. The flattening of the X-ray profile, rather than contradicting this model, might actually be consistent with it. Only high-resolution spatial and spectral X-ray images of this cluster's center will definitively settle this issue.

7. SUMMARY

This paper seeks to explain the origin of the line-emitting nebulosity seen at the centers of some clusters of galaxies. We present a simple model for the photoionization of cool (10^4 K), filamentary clouds of varying column density by radiation from a hot, confining medium cooling from 10^7 K. This model succeeds in reproducing the range of emission line ratios observed and suggests that some clusters contain thick 10^{21-22} cm^{-2} clouds, while in others only thin 10^{17-18} cm^{-2} clouds are present. We postulate that these clouds are the condensates that have formed in the central regions of a cooling flow where the flow velocities are close to the sound speed in the hot gas. The luminosities, surface brightnesses, and line broadenings expected from such a region agree well with the observed characteristics of the emission-line nebulae. The most luminous Hα emitters require a flow of ~300 $M_\odot$ yr^{-1} into a 10 kpc radius, yet this high a flow rate does not necessarily contradict the observed velocity dispersions and X-ray surface brightness profiles. In NGC 1275 at the center of the Perseus cluster, soft X-ray absorption by the condensates can lead to X-ray surface brightness flattening, and an active nucleus might dominate the photoionization within a 2 kpc radius.

At worst, this model provides a convenient framework in which to analyze these nebulae because it succeeds in explaining line ratios that low-velocity shocks and AGN photoionization do not. However, if the nebulae really are self-irradiated condensing regions, this model can be used as a stepping stone to begin to answer other questions about cooling flows, such as: How do cooling flows evolve? Do magnetic pressures and turbulence affect the formation of filaments? Are the filaments sites for star formation? And, of course, what form does all that mass take after it drops out of the flow? With optical narrow-

band imaging, long-slit spectroscopy, and improved spatial and spectral resolution X-ray observations, we can begin to probe for the answers to these questions.

We thank John Stocke, Mike Shull, Andy Fabian, Chris McKee, and Scott Tremaine for enlightening conversations, Gary Ferland and John Raymond for providing their software, and Stefi Baum for providing her line ratios. We would also like to acknowledge support from the NASA Astrophysical Theory Program (NAGW-766), the NASA Graduate Student Researchers' Program, NSF grant AST 87-15983, and Zonta International for an Amelia Earhart Fellowship (M. D.).

REFERENCES

Arnaud, K. A. 1988, in Cooling flows in Galaxies and Clusters, ed. A. Fabian (Cambridge: Cambridge University Press), 31
Balbus, S. A., & Soker, N. 1989, ApJ, 341, 61
Baldwin, J. A., Phillips, M. M., & Terlevich, R. 1981, PASP, 93, 5
Baum, S. 1987, Ph.D. thesis, University of Maryland
Baum, S., & Heckman, T. 1990, ApJ, in press
Begelman, M., & Fabian, A. C. 1990, MNRAS, 244, 26P
Binette, L., Dopita, M. A., & Tuohy, I. R. 1985, ApJ, 297, 476
Branduardi-Raymont, T., Fabricant, D., Feigelson, E., Gorenstein, P., Grindlay, J., Soltan, A., & Zamorani, G. 1981, ApJ, 248, 55
Burns, J. O. 1990, AJ, 99, 14
Canizares, C. R., Clark, G. W., Jernigan, J. G., & Markert, T. H. 1982, ApJ, 262, 33
Canizares, C. R., Clark, G. W., Markert, T. H., Berg, C., Smedira, M., Bardas, D., Schnopper, H., & Kalata, K. 1979, ApJ, 234, L33
Canizares, C. R., Markert, T., & Donahue, M. 1988, in Cooling Flows in Clusters of Galaxies, ed. A.C. Fabian (Dordrecht: Reidel), 63
Canizares, C. R., Stewart, G. C., & Fabian, A. C. 1983, ApJ, 272, 449
Cowie, L. L., & Binney, J. J. 1977, ApJ, 215, 723
Cowie, L. L., Hu, E. M., Jenkins, E. B., & York, D. G. 1983, ApJ, 272, 29
Diaz, A. I., Pagel, B. E. J., & Terlevich, E. 1985, MNRAS, 214, 41P
Diaz, A. I., Pagel, B. E. J., & Wilson, I. R. G. 1985, MNRAS, 212, 737
Draine, B. T., & Lee, H. M. 1984, ApJ, 285, 89
Dreher, J. W., Carilli, C. L., & Perley, R. A. 1987, ApJ, 316, 611
Edge, A. C., & Stewart, G. C. 1991, MNRAS, submitted
Fabian, A. C., Hu, E. M., Cowie, L. L., & Grindlay, J. 1981, ApJ, 248, 47
Fabian, A. C., & Nulsen, P. E. J. 1977, MNRAS, 180, 479
Fabian, A. C., Nulsen, P. E. J., & Canizares, C. R. 1982, MNRAS, 201, 933
———. 1984, Nature, 310, 733
Ferland, G. J. 1989, OSU Internal Report 89-001
Ferland, G. J., & Netzer, H. 1983, ApJ, 264, 105
Ferland, G. J., & Osterbrock, D. E. 1985, ApJ, 289, 105
Gaetz, T. J., & Salpeter, E. E. 1983, ApJ, 52, 155
Gorenstein, P., Fabricant, D., Topka, K., Harnden, F. R., Jr., & Tucker, W. 1978, ApJ, 224, 718
Gorenstein, P., Fabricant, D., Topka, K., Tucker, W., & Harnden, F. R. 1977, ApJ, 216, L95
Heckman, T. M. 1981, ApJ, 250, L59
Heckman, T. M., Baum, S. A., van Breugel, W. J. M., & McCarthy, P. 1989, ApJ, 338, 48 (HBvM)
Henriksen, M. J. 1985, Ph.D. thesis, University of Maryland
Henriksen, M. J., & Mushotzky, R. F. 1986, ApJ, 292, 441
Hu, E. M., Cowie, L. L., & Wang, Z. 1985, ApJS, 59, 447
Johnstone, R. M., & Fabian, A. C. 1988, MNRAS, 233, 581
Johnstone, R. M., Fabian, A. C., & Nulsen, P. E. J. 1987, MNRAS, 224, 75 (JFN1987)
Jones, C., & Forman, W. 1984, ApJ, 276, 38
Kato, T., Tabara, H., Inoue, M., & Aizu, K. 1987, Nature, 329, 223
Kent, S. M., & Sargent, W. L. W. 1979, ApJ, 230, 667
Loewenstein, M. 1989, MNRAS, 238, 15
Loewenstein, M., & Fabian, A. C. 1990, MNRAS, 242, 120
Lynds, R. 1970, ApJ, 159, L151
McNamara, B. R., & O'Connell, R. W. 1989, AJ, 98, 2018
Minkowski, R. 1957, in IAU Symposium 4, Radio Astronomy, ed. H. C. van der Hulst (Cambridge: Cambridge University Press), 7
Mitchell, R. J., Culhane, J. L., Davison, P. J., & Ives, J. C. 1979, MNRAS, 189, 329
Mushotzky, R. F., Serlemitsos, P. J., Smith, B. W., Boldt, E. A., & Holt, S. S. 1978, ApJ, 225, 21
Nulsen, P. E. J. 1986, MNRAS, 221, 337
O'Dea, C. P., & Baum, S. 1987, in Radio Continuum Processes in Clusters of Galaxies, ed. C. O'Dea & J. Ulson (Charlottesville: NRAO), 141
Osterbrock, D. E. 1989, Astrophysics of Gaseous Nebulae and Active Galactic Nuclei (Mill Valley, CA: University Science Books)
Owen, F. N., Ge, J. P., Eilek, J. A., & Keel, W. C. 1989, in Clusters of Galaxies: A Collection of Posters, ed. M. J. Fitchett & W. R. Oegerle (Baltimore: STScI), 209
Raymond, J. C., Cox, D. P., & Smith, B. W. 1976, ApJ, 204, 290
Raymond, J. C., & Smith B. W. 1977, ApJS, 35, 419
Romanishin, W., & Hintzen, P. 1988, ApJ, 324, L17
Sarazin, C. L. 1988, X-Ray Emission from Clusters of Galaxies (Cambridge: Cambridge University Press)
Savage, B. D., & Mathis, J. S. 1979, ARA&A, 17, 73
Shields, J. C., & Filippenko, A. V. 1990, ApJ, 353, L7
Shull, J. M., & McKee, C. F. 1979, ApJ, 227, 131
Soker, N., & Sarazin, C. L. 1990, ApJ, 348, 73
Stern, R., Wang, E., & Bowyer, S. 1978, ApJS, 37, 195
Stewart, G. C., Fabian, A. C., Jones, C., & Forman, W. 1984, ApJ, 285, 1
Thomas, P. A., Fabian, A. C., & Nulsen, P. E. J. 1987, MNRAS, 228, 973
Tribble, P. 1991, MNRAS, 248, 741
Voit, G. M., & Donahue, M. 1990, ApJ, 360, L15 (Paper I)
White, R. E., & Sarazin, C. L. 1987a, ApJ, 318, 612
———. 1987b, ApJ, 318, 629
———. 1988, ApJ, 335, 688